Sustainable Energy & Fuels

Interdisciplinary research for the development of sustainable energy technologies

Accepted Manuscript

This article can be cited before page numbers have been issued, to do this please use: A. S. Rajpurohit, V. R. M. Talla, M. Jaccob, K. Kr and B. Viswanathan, *Sustainable Energy Fuels*, 2023, DOI: 10.1039/D3SE00131H.

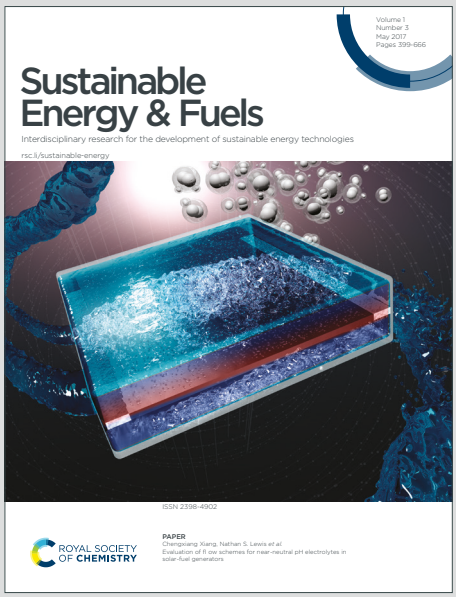

ROYAL SOCIETY OF CHEMISTRY

rsc.li/sustainable-energy

Aqueous Phase Hydrogenation of Furfural on Ni/TiO_2 Catalysts: Nature of Support Phase Steers the Product Selectivity

Anil Singh Rajpurohit,[a,b] Venkata Rama Mohan Talla,[c] Madhavan Jaccob,[a*] Krishnamurthy Konda Ramaswamy[b*] and Balasubramanian Viswanathan[b*]

[a] Department of Chemistry & Loyola Institute of Frontier Energy (LIFE), Loyola College(Affiliated to University of Madras), Chennai-600034, India
[b] National Centre for Catalysis Research, IIT Madras, Chennai-600036, India
[c] Department of Chemistry, AdikaviNannaya University-Tadepalligudem Campus, Tadepalligudem -534101, India

ASTRACT

Nickel catalysts supported on six different titania phases (ATA, ATH, P25, ART, RTH and RTS), that differ in phase composition (anatase/rutile), textural characteristics, acidity and nature of metal support interactions, have been investigated for aqueous phase hydrogenation of furfural. The two phases of titania, anatase and rutile, showed remarkable differences in the activity as well as selectivity for products. Higher conversion of furfural was observed on rutile phase supported catalysts. While both phases showed the formation of furfuryl alcohol, on anatase supported catalysts formation of deep hydrogenated products was restricted to cyclopentanone only. On the other hand, on rutile phase supports, further hydrogenated products, like, tetrahydrofurfuryl alcohol and cyclopentanol were observed. Activity/selectivity patterns are rationalized on the basis of metal-support interactions based on XPS, DFT, H_2-TPR and acidity data. The results showed that the reducibility of support depends on titania crystal phase, which effect active sites at interface and on metal surface charge redistribution and blockage of reactive sites. The higher reducibility of anatase phase was found to be detrimental for hydrogenation activity. This investigation paves way for designing catalysts for selective catalytic transformations of bio-renewable raw materials, like furfural.

Keywords: Furfural, Nickel catalyst, TiO_2 phases, Hydrogenation, Ring rearrangement

1. Introduction

Lignocellulosic biomass is regarded as a sustainable and environmentally benign feedstock substitute for fossil-based raw materials, for the production of chemicals and fuels[1]. Liquefaction process such as pyrolysis or hydrothermal treatment, is carried out to break down the solid polymeric structure of biomass[2–4]. In general, biomass-derived molecules are highly functionalized and contain higher amount of oxygen than petrochemicals[5]. Therefore, the selective catalytic hydrogenation process is of immense research interest for value addition of bio-derived initial stage platform molecules.

Noble metals from Pt group and the non-noble metals like Ni, Cu, Coas active phases, have been extensively studied to improve the activity towards selective/partial hydrogenation of unsaturated organic compounds[6,7]. Furfural (Furan-2-carbaldehyde) has been identified as one of the key platform molecules, which is derived from pentosan rich agriculture residues like oats hull, corncobs, bagasse, rice husk, cotton husk, etc., by hydrolysis and dehydration process[8]. It can be transformed into a wide variety of highly useful chemical intermediates, such as, furfuryl alcohol, tetrahydrofurfuryl alcohol, 2-methylfuran, cyclopentanone, cyclopentanol, pentanediols, etc., through hydrogenation, hydrodeoxygenation, hydrolysis, and rearrangement reactions. They are used for wide range of applications, such as plasticizer, hypergolic propellent, production of thermoset polymer and foundry resins, fuel additive and green solvent, in the production of fragrance and flavour, etc.,[9–13]. Further transformation of furfural into easily separable or desired products in aqueous medium will be a cost-effective process.

Several parameters of the metals and supports, such as, the size, shape, exposed facets, selective blocking of sites, alloying, temperature treatment used in the synthesis of

catalysts etc., are known to influence the activity and selectivity of a reaction as they are prone to modify the electronic properties of the catalysts[14–17]. Bernal et al. observed that the amount of hydrogen adsorption on Pt/CeO_2 catalysts decreased with increase in reduction temperature[18]. Abid et al. found that the Pt/CeO_2catalysts prepared from platinum nitrate at high reduction temperature have transformed to intermetallic compound (CePt5) resulting in change of crotonaldehyde hydrogenation selectivity from C=C towards C=O group. On other hand, use of chloride precursor prevented metal-support interaction and therefore C=C hydrogenation was preferred on Pt nanoparticles[19].

Among various oxides supports, titania was found to withstand severe hydrothermal conditions[20]. Its redox nature and surface functionalities can tune metal-support interaction and therefore influences the selectivity of partially hydrogenated products. For example, Ru grows preferably on rutile in mixed phase TiO_2, whereas Pt was found to be randomly distributed over both anatase and rutile phases of the support. The stronger interaction of Ru with rutile phase was found to be beneficial for levulinic acid hydrogenation[21]. Similar observation was made for xylose hydrogenation where stronger interaction and dispersion of Ru nanoparticles was attributed to lattice matching/epitaxial growth of RuO_2 with rutile TiO_2 surface, which provided higher activity and selectivity to xylitol than on anatase catalyst[22]. In guaiacol hydrogenation, the partially reduced anatase support found to migrate over Ni nanoparticle to form TiO_x overlayer, generating highly selective catalytic sites for hydrodeoxygenation[17].

TiO_2 supported catalysts have shown improved selectivity for furfural hydrogenation[23–27].In comparison to rutile support, the strong interaction between TiO_x and Ru nanoparticle on anatase support formed at higher reduction temperature and further alloying with Co have shown increase inactivity and selectivity to furfuryl alcohol[28]. Commercial Raney Ni catalyst is found to be less active than supported catalysts[29]. Ni supported on anatase TiO_2, when

alloyed with Co, displays higher selectivity to cyclopentanone. Same Ni-Co catalyst preparedat higher pH, enhanced the metal-support interaction, which changes the reaction route of furfuryl alcohol intermediate, from ring rearrangement to ring hydrogenation path, forming tetrahydrofurfuryl alcohol as major product[30].However, on Ni-NiO/P25 catalyst, the synergy between Ni-NiO was proposed to favour cyclopentanone selectivity in aqueous phase furfural hydrogenation, whereas on pure phase supports or on the chemically reduced Ni the activity declines[31].Recent study on 5-hydroxymethylfurfural, an analogue to furfural have shown that the Ni catalyst with higher concentration of acidic sites on TiO_2 (P25 and P90) support would yield both hydrodeoxygenation and ring hydrogenation products in dioxane, while the anatase with lower acidity and higher Ni dispersion selectively favoured hydrodeoxygenation products[32].

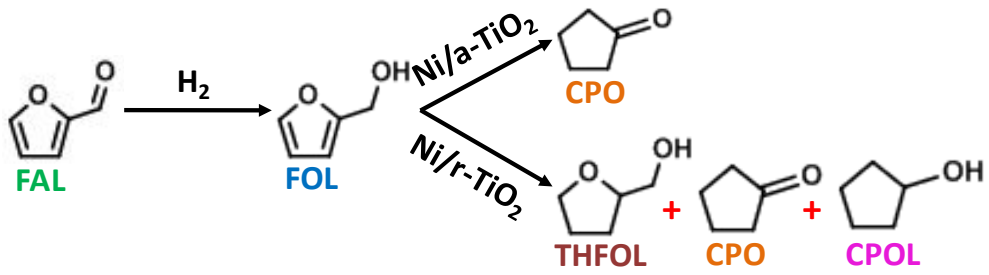

Scheme 1. Aqueous phase hydrogenation of furfural over Ni/TiO_2 catalyst.[FAL =furfural; FOL = furfuryl alcohol; CPO = cyclopentanone; THFOL=tetrahydrofurfuryl alcohol; CPOL = cyclopentanol]

The crystal phases and morphologies of support, due to different physico-chemical properties, can play an important role in catalysing furfural transformations. Even though there are several studies on furfural hydrogenation over supported Ni catalysts, the influence of phase composition of TiO_2 support on the electronic properties of Ni nanoparticles and metal-support interactions have not been studied in detail. In this work Ni catalysts supported on different TiO_2 polymorphs (anatase/rutile) with different compositions were synthesized by

View Article Online
DOI: 10.1039/D3SE00131H

wet impregnation method and further characterized by various physico-chemical characterization techniques to explain the relationships between titania phase and the catalytic properties. Our results show that pure anatase phase-based catalysts display low activity than rutile containing catalysts, but remain highly selective towards hydrogenated products.

2. Results and Discussion

The Ni catalysts synthesized using commercial anatase titania obtained from Aldrich and Hombikat are labelled as ATA and ATH, whereas the catalysts with anatase-rutile mixed phase titania supports obtained from EVONIK and Aldrich are labelled as P25 and ART. Additionally, two catalysts supported on rutile titania synthesized from hydrothermal and sol-gel method are labelled as RTH and RTS. About 5 wt% Ni content was loaded on these supports by impregnated method, followed by calcination in air at 450°C for 4 h, and then reduction in H_2 flow at 450°C for 4 h. The prepared catalyst were further characterised to account for the reactivity of the catalyst. The detailed catalyst preparation methods and characterization tools used are given in the supplementary information file.

a. X-ray diffraction

X-ray diffraction patterns of Ni/TiO_2 catalysts with different phases and compositions of titania are shown in Figure 1a-b. The main diffraction peaks at *ca.*2θ = 25.3°, 37.9°, 48.0°, 53.9°, 55.1° and, 62.7° were indexed to (101), (004), (200), (105), (211) and, (204) facets of anatase phase (JCPDS no. 21-1272), whereas the reflections at27.4°, 36.1°, 39.2°, 41.3°, 44.1°, 54.3°, 56.6°, 62.8°, 64.1°, 69.0° and, 69.8° corresponding to (110), (101), (200), (111), (210), (211), (220), (002), (310), (301) and, (112) indices reveal the presence of rutile phase (JCPDS no. 75-1753). The phase transformation from anatase to rutile occurs at temperatures above 500°C[33]. In ATA and ATH based catalysts, no rutile peaks were found after calcinations and reduction process, indicating their thermal stability. For RTH and RTS

samples, the peaks corresponding to rutile phase were detected. The most predominant crystallographic plane (101) and (110) due to anatase and rutile phases were used to calculate the phase composition of the titania (Table 1)[34]. The rutile content in the mixed phase supports of P25 and ART catalysts was found to be 23 and 51% respectively. On reduction at 450 °C, the NiO phase on all supports reduced to metallic Ni. Due to either high dispersion and/or low metal loading, only weak Ni (111) peak was observed at *ca.* 44.5° (JCPDS no. 04-0850)

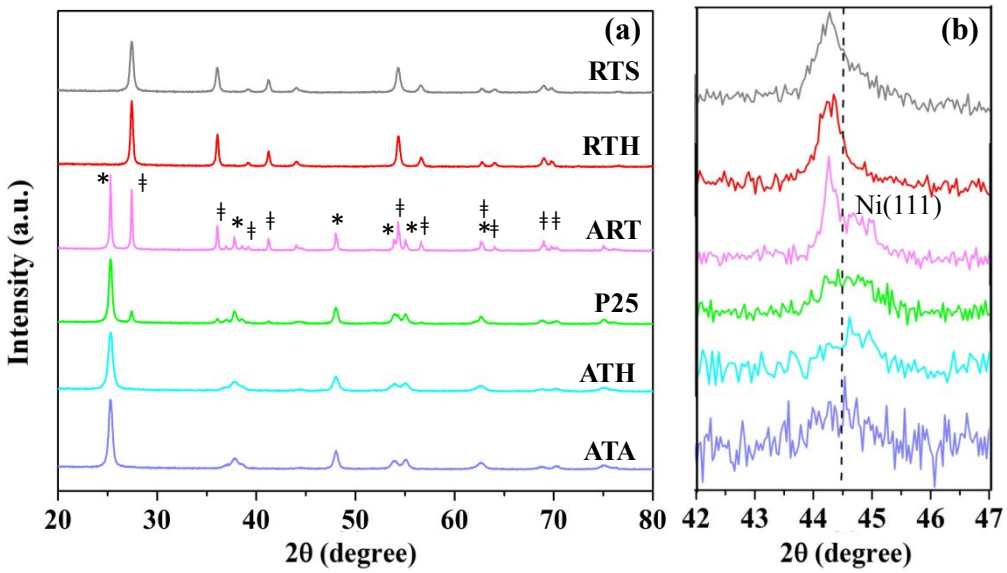

Figure 1. (a) X-ray diffractograms of the 5 wt% Ni/TiO_2catalysts with different anatase (*) and rutile (ǂ) composition (b) Magnified zone of the Ni(111) reflection. * and ‡ denotes anatase and rutile phase, respectively.

for ATA, ATH and, P25 catalysts (given in Table 1). On the other hand, due to the overlap of Ni (111) peak with TiO_2 rutile (210) peak, it was difficult to distinguish the metallic nickel on catalysts with rutile phase (ART, RTH and, RTS). Also, no additional peaks corresponding to $NiTiO_3$ or NiO were found (Figure S1).

b. Electron microscopy

View Article Online
DOI: 10.1039/D3SE00131H

Surface morphologies of synthesized catalysts are shown in Figure 2a-f. Both anatase based catalysts exhibit fine particles of size around 50 nm and below, which agglomerated into large clusters. It can be seen from the micrograph that support ATH catalyst exhibits small nanoplates like morphology. Such regular shapes are not observed for ATA. The P25 sample shows granular nanoparticles between 30-50 nm without agglomeration. However, support of ART catalyst shows large spherical particles of about 100-350 nm in diameter along with distinguishable small particle clusters. It is noted that the surface morphology of particles appears smoother with increase in size. The particles of both rutile supports (RTS and RTH) show small rod shapes of about 50 to 200 nm in length

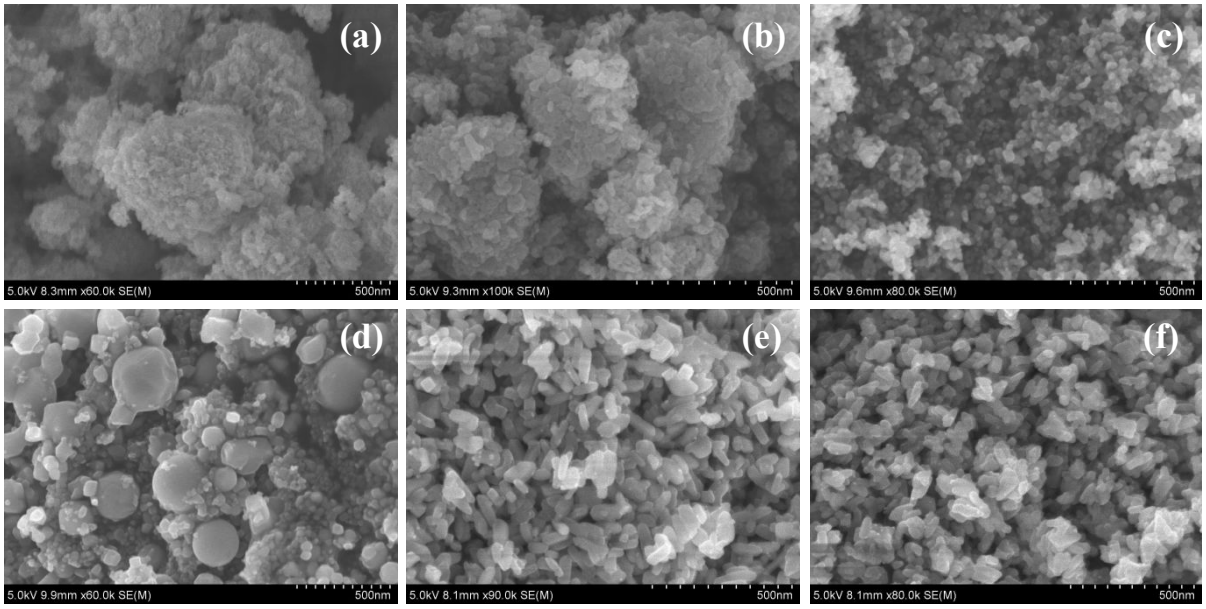

Figure 2. SEM micrographs of Ni catalysts supported on different polymorphs of TiO_2: (a) ATA, (b) ATH, (c) P25, (d) ART, (e) RTH and, (f) RTS.

Elemental mapping carried out by Energy Dispersive X-ray spectroscopy (Fig. S1) shows uniform distribution of Ni over all TiO_2 supports indicating successful synthesis of supported catalysts. Elemental analysis of all catalysts (in Table 1) by AAS shows actual Ni loading

varies between 4.5 to 4.9 wt%, confirming that almost all Ni precursor impregnation on titania support during synthesis.

TEM images of Ni nanoparticles supported on titania are shown in Figure 3. The size of Ni nanoparticles loaded over titania supports do not correlate with their BET surface area. In case of ART catalyst that has surface area nearly equal to rutile catalysts, the Ni nanoparticles size has increased to 15 nm.

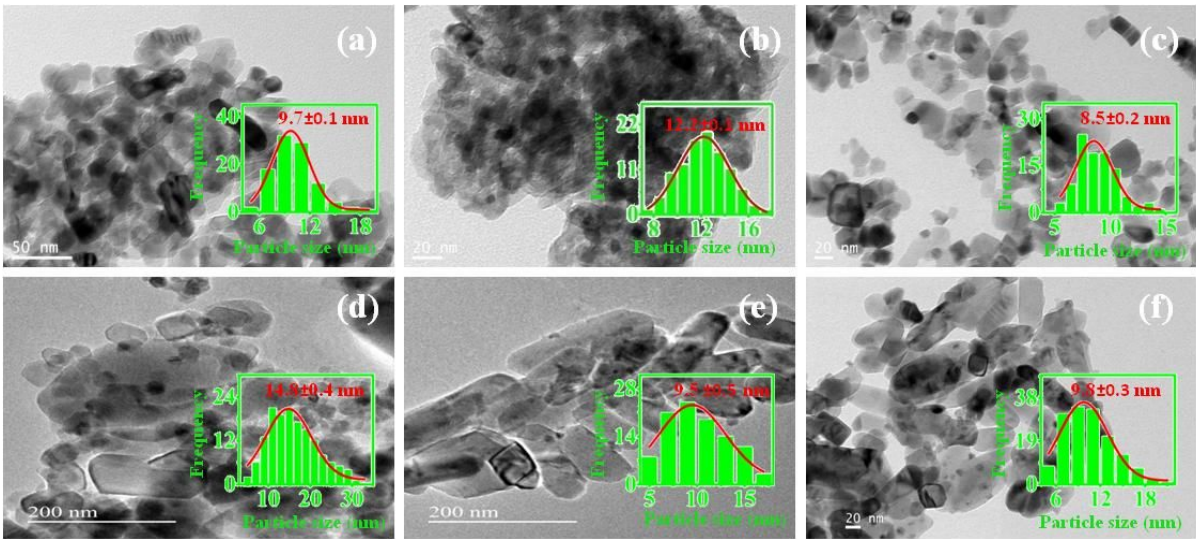

Figure 3. TEM images and histograms(inset)of Ni nanoparticles supported on (a) ATA, (b) ATH, (c) P25, (d) ART, (e) RTH and, (f) RTS catalysts.

On other hand, the nanoparticles on rutile supports were found dominantly around 10 nm. Of all the catalysts, the smaller particles were obtained over P25 catalyst. This difference is likely due to high surface area of P25 compared to other rutile supports. In contrast, for anatase supports, despite of having high surface area, the Ni particles are larger in size, in the range of 10 to 12 nm. Even the larger grain boundaries of anatase supports due to their smaller crystallites (Table S1) does not provide any additional benefit to stabilize smaller nanoparticles. From this it can be inferred that the Ni particle growth depends on other textural properties of support such as anchoring of Ni species by surface hydroxyls, their

densities, nature of nucleation sites, etc., It also leads to the conclusion that rutile phase plays an important role in anchoring Ni nanoparticles.

Table 1. Physico-chemical properties of Ni catalysts

Catalyst	Ni (%)[a]	D_{Ni} (nm)[b]	Ni Particle size (nm)[c]	Ni dispersion (%)[d]	Total H_2 (µmol/g)[e]	Strength of acidic sites (µmol/g)[f]				Density of acidic sites (µmol/m²)[g]
						Weak	Medium	strong	total	
ATA	4.60	7.8	9.7	10.4	841	140	42	49	231	3.7
ATH	4.51	12.1	12.2	8.3	969	156	69	61	286	4.3
P25	4.82	8.1	8.5	11.9	701	77	55	73	205	5.1
ART	4.93	12.4	14.8	6.8	796	53	21	35	109	4.7
RTH	4.89	-	9.5	10.6	726	60	22	48	130	5.9
RTS	4.71	-	9.8	10.3	765	49	34	26	109	4.7

[a]Ni content from AAS;[b]averagecystallite size of (111) plane of nickel nanoparticle calculated using Scherrer equation;[c]obtained from TEM ;[d]Dispersion of nickel on titania calculated using TEM particle size;[e]obtained from H_2-TPR analysis;[f]obtained from NH_3-TPD analysis;[g]ratio of amount of acid sites/BET surface area

c. Textural analysis

Nitrogen adsorption-desorption isotherms and the pore size distribution data obtained for reduced catalyst samples are shown in Figure S3 and their physico-chemical properties are given in Table S1.All samples show type IV isotherm with H3 hysteresis loop, demonstrating meso porous nature of the samples. Both ATA and ATH catalysts displayed hysteresis from 0.6 to 1 P/P_o, where the loop part at lower relative pressure present adsorption-desorption process taking place in voids formed between smaller anatase TiO_2 nanoparticles and closer to unity is due to larger voids present in between agglomerated clusters as observed in SEM images. The remaining four samples containing pure rutile or mixed phases showed hysteresis at p/p_0 close to unity. The large voids present in between these particles gives pore size distribution in meso and macropores ranges. BET surface area of pure anatase supported catalysts is considerably higher as compared to rutile and mixed phases catalysts.

d. Temperature programmed reduction

TPR profiles of supported NiO catalysts are displayed in Figure 4a, wherein H_2 consumed by the calcined samples during reduction is measured as a function of temperature. A preliminary examination of the peaks shows that the nickel supported on anatase supports are

reduced at lower temperatures, compared to the nickel supported on rutile titania. The reduction temperature increases with the percentage of rutile phase in the titania samples.

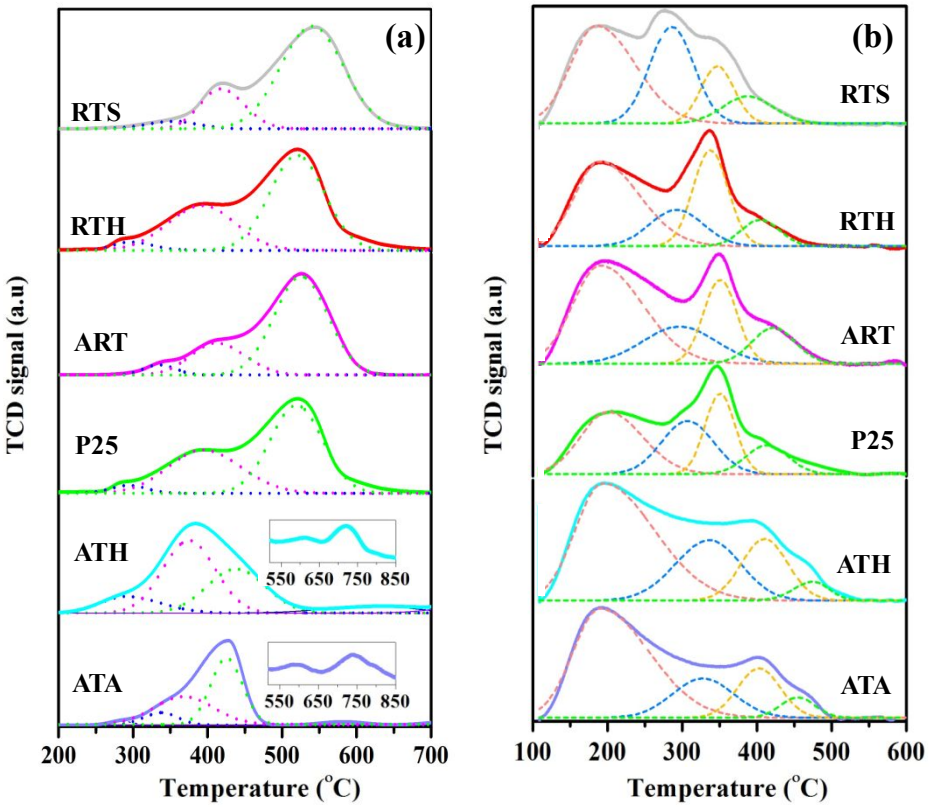

Figure 4. (a) H_2-TPR profiles of NiO supported on different titania supports and (b) NH_3TPD profilesfor the acid sites of reduced Ni/TiO_2catalysts.

NiO supported on ATA and ATH samples start reducing at *ca.* 250°C and maximum H_2consumption (T_{max}) is observed at 400-428°C respectively. On the other hand, for the mixed phases (P25 and ART) and rutile phases (RTH, RTS) supported nickel catalysts, the major reduction peak temperature is shifted to 460-525 °C, with a minor peak between 320 and 425 °C. Also, for the anatase supported catalysts a peak above 650 °C is observed, which is not present for the mixed phases and rutile samples (see inset of Figure 4a). The H_2 consumption given in Table 1 suggests that anatase phase supported catalysts consumes higher amount of hydrogen than the rutile phase supported catalysts. These results show characteristic influence of rutile phase on Ni reduction even when it is present at lower

View Article Online
DOI: 10.1039/D3SE00131H

concentrations. When supported on rutile phase, NiO reduction occurs at higher temperatures, which is due to stronger NiO interaction with rutile compared to anatase phase. This was seen even with P25 catalyst where the rutile phase composition was lower. Secondly, the excess hydrogen that was consumed by the anatase catalyst, than needed for reduction of complete NiO to metallic Ni, is used to reduce TiO_2 [35].

e. Surface acidity

The qualitative and quantitative number of acidic sites plays a significant role in the catalytic transformation of furfuryl alcohol to cyclopentanone[36–39]. The surface acidity of Ni catalysts was determined by NH_3-TPD and the resulting profiles are shown in Figure 4b. The composite peaks obtained were deconvoluted into three peaks consisting of weak, medium and strong acidic sites at temperatures respectively at *ca.*180-230°C, 230-350°C and above 350°C. The distribution of acidic sites, total sites, and their density on catalyst surface are summarized in Table 1 and corresponding temperatures in Table S2. As the rutile percentage is increased, the peak positions are shifted to lower temperature regions. Anatase samples show high intensity peak in the low temperature region at *ca.*180-200°C revealing the presence of high amount of weak acidic sites. On the other hand, in addition to major peak corresponding to weak acid sites on mixed and rutile phase samples, a predominant peak emerged at high temperature (*ca.*350°C along with a shoulder peak at 413°C) representing stronger acidic sites. Therefore, for rutile containing samples, the main contribution to total acidity comes from both these acidic sites. The medium strength acidity peaks are present in between weak and strong desorption peaks and is clearly visible for RTS at *ca.* 286°C. The total acidity of the anatase catalysts was higher than that of the rutile catalysts. This difference is due to high surface area of the anatase supports, which has significantly more accessible acidic sites even after dispersion of Ni nanoparticles.

f. X-ray photo electron spectroscopy

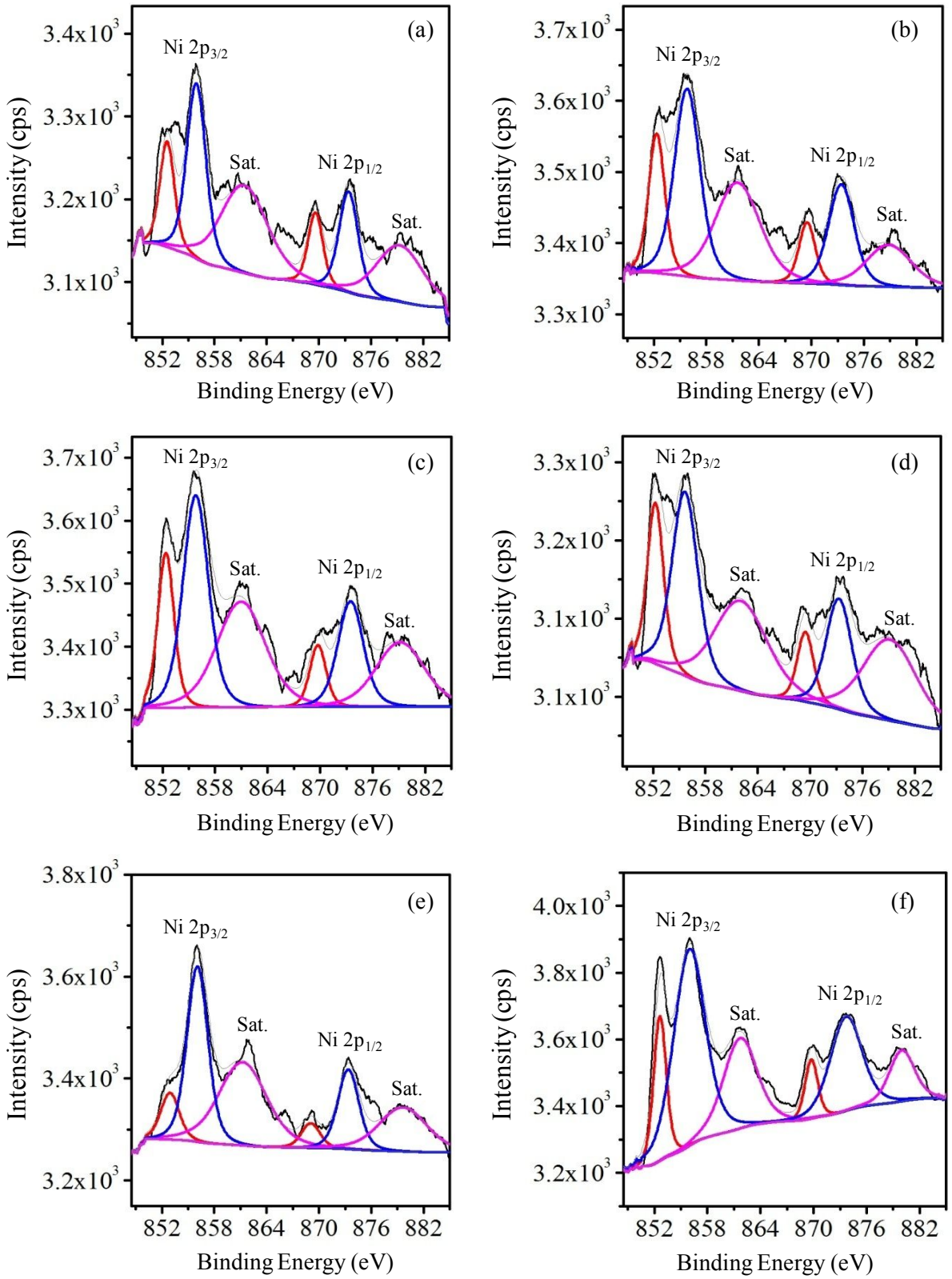

Figure 5. Ni 2p core level XP spectra for the Ni catalysts supported on (a) ATA, (b) ATH, (c) P25, (d) ART, (e) RTH and, (f) RTS.

View Article Online
DOI: 10.1039/D3SE00131H

X-ray photoelectron spectroscopy analyses were carried out to gain insights into metal support interaction and its influence on surface electronic properties. Figure 5 shows the nickel 2p core level XPS of the prepared catalysts and the corresponding binding energies and atomic ratio of elements are given in Table S3. Although, the reduced catalysts were introduced for analysis, the nickel gets partially oxidised during the transfer of the samples from tubular furnace to the sample holder. As a result, we could only get the mixture of both Ni^0 and Ni^{2+} peaks that was distributed over 852-879 eV and this was deconvoluted into $Ni2p_{3/2}$ and $Ni2p_{1/2}$ peaks. The peak at ~852 and ~869 eV was attributed to Ni^0 state and the others at ~856 and ~873 eV were assigned to Ni^{2+} state[40]. The $Ni2p_{3/2}$ and $Ni2p_{1/2}$ peak splitting is ~17.3 eV, whereas for titania it is around 5.7 eV. The values given in the Table S3 show that as the percentage of rutile is increasing the Ni/Ti surface ratio also increases. In general, surface area of support, Ni nanoparticles dispersion, the presence of larger Ni nanoparticles, evolving of reduced support onto the catalyst surface, etc, contribute to the surface Ni/Ti atomic ratio[41,42]. As seen from Figure 5 and Table S3, the samples RTH and RTS are having Ni^0 peaks at 852.6 and 852.5 eV, respectively. Notably, the Ni^0 peak for mixed phases are shifted to relatively lower binding energy as the anatase percentage increases with ART catalyst showing peak at 852.4 eV and P25 sample at 852.3 eV. The binding energy is further lowered to 852.2 eV for anatase supported catalysts (ATH and ATA), indicating charge redistribution between metal and support. The Ti 2p spectra in Figure S4 show two peaks at ~457 and ~458 eV corresponding to Ti^{3+} and Ti^{4+} state, respectively. The $\frac{Ti^{3+}}{(Ti^{3+}+Ti^{4+})}$ atomic ratio increases gradually with anatase composition of catalyst, suggesting the enhancement of support reducibility, which can influence metal-support interaction. Figure S5 shows the deconvoluted O1s core level spectra of the prepared catalysts. The three peaks are associated with oxygen bonded to the metal lattice site, surface hydroxyl group and the adsorbed water or oxygen[43].

View Article Online
DOI: 10.1039/D3SE00131H

g. Aqueous phase hydrogenation of furfural

The prepared catalysts are screened for the hydrogenation of furfural (FAL) in aqueous phase (see scheme 1). The conversion and selectivity results obtained at two different temperatures over catalysts with different supports are shown in Figure 6. It can be seen from these results that the rutile supported catalysts shows better activity than anatase based catalysts. At 100°C reaction temperature, furfuryl alcohol (FOL) is the major product over all catalysts. Both ATA and ATH catalysts showed 95.6 and 94.3% selectivity to FOL, respectively. A small amount of cyclopentanone (CPO, <5%) is also seen on both these anatase catalysts. However, the FOL selectivity decreases on mixed phase and rutile catalysts, due to the further hydrogenation of furfuryl alcohol. The deep hydrogenated products such as tetrahydrofurfuryl alcohol (THFOL, <6%) and cyclopentanol (CPOL, ~1%) were the additional products identified on these supports.

View Article Online
DOI: 10.1039/D3SE00131H

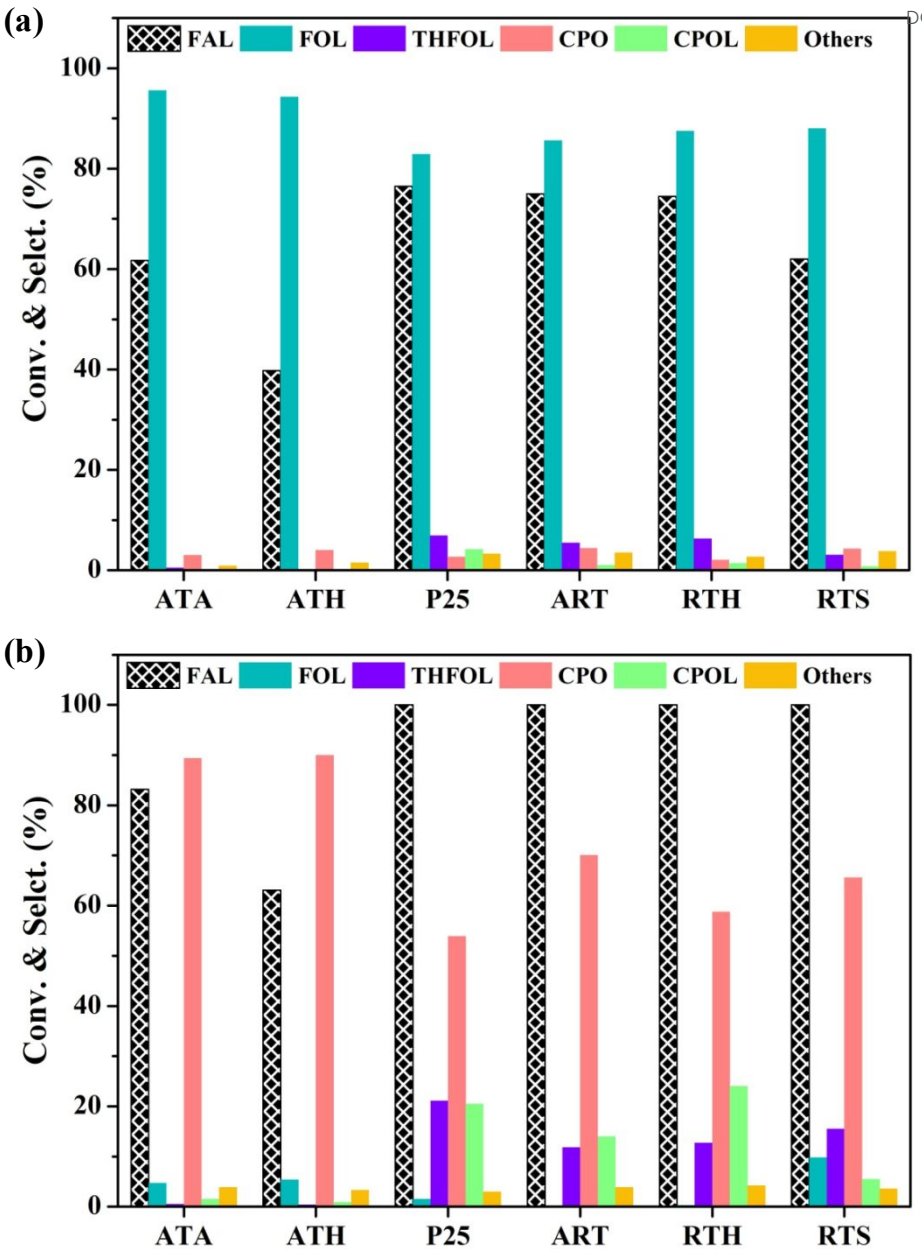

Figure 6. Furfural hydrogenation over Ni catalysts with different supports at (a) 100°C and (b) 140°C. Reaction conditions: 5.2 mmol furfural, 50 mL water, 50 bar H_2, 4h, 500 rpm.

The increase in the conversion from 39.8% on ATH to 61.7% on ATA does not have much effect on their FOL selectivity. Similar behaviour was observed between rutile catalysts, where the FAL conversion increases from 62% on RTS to 74.5% on RTH catalyst maintaining FOL selectivity of 88%.

It is also found that the ring hydrogenated product such as THFOL formed on RTH catalyst with 6.3% selectivity got suppressed to 3.1% on RTS catalyst at the cost of increase in CPO

and other unidentified products. Similar observation is made on mixed phase catalysts except that the decrease in seen in FOL selectivity instead of THFOL. Both P25 and ART catalysts were able to achieve activity identical to RTH catalyst. Hence, these results demonstrate that the rutile phase, even at low composition in support (P25) has influenced product distribution. To get further insight into catalytic activity of rutile phase, the reaction conditions were optimized using RTH catalyst. Figure7a shows influence of hydrogen pressure on the activity of RTH catalyst. The product distribution selectivity does not alter much with change in pressure, but the activity increases from 65.7% at 40 bar to 76.9% at 60 bar. Hence, 50 bar at which conversion reaches 74.5% is taken as optimum pressure.

In order to understand the role of acidic sites and solvent, the reaction in water was compared with that in isopropanol. The isopropanol is known for hydrogen donor ability[44,45]. But under the given reaction conditions, in presence of isopropanol, FAL conversion is suppressed to 40.6% vis-à-vis 74.5% in water medium. FOL is selectively formed (87.5%) in water (Fig. 7b), but in isopropanol its selectivity decreases by 60.4%,with the formation of complete hydrogenation product, THFOL, with 31.2% selectivity. Though hydrogen has high solubility in isopropanol than water, the water was able to activate polar carbonyl bond by hydrogen bonding and also provides additional water mediated routes with low energy barrier for hydrogenation[46]. Also, no ring rearrangement takes place in alcohol medium suggesting that proton from dissociated water at acidic sites is necessary to generate protonated furfuryl alcohol, the intermediate species to form cyclopentanone[47].

View Article Online
DOI: 10.1039/D3SE00131H

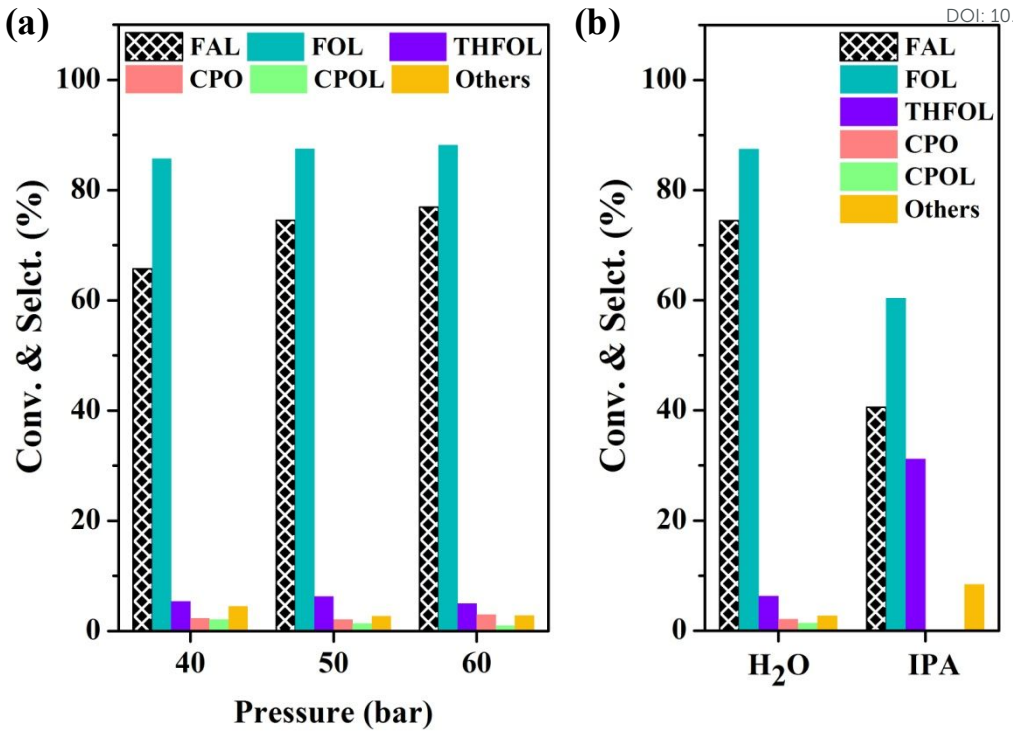

Figure 7. Furfural hydrogenation over RTH catalysts (a) at different pressure and (b) in different solvents (50 bar H_2). Reaction conditions: 5.2 mmol furfural, 50 mL water, 100°C, 4h, 500 rpm.

The degree of hydrogenation with respect to time is given in Figure 8. After 2h of reaction, the conversion reaches 62.5% and increases with time up to 99.4% after 8h. The initial selectivity 90% for FOL has decreased to 56.3%. The CPO selectivity has increased twice than that of THFOL. At lower reaction temperature CPOL formation is not favoured (~1% selectivity). Therefore, reaction time of 4h is desirable to obtain FOL selectivity with minimum side products.

When the reaction temperature is raised to 140°C, as shown in Figure 6b, FOL undergoes ring rearrangement to CPO on all catalysts. The protonated intermediates formation in aqueous phase and the subsequent transformations are catalysed by acidic sites[48,49]. However, the nickel catalysts supported on pure anatase titania has resulted in only formation of CPO, whereas on mixed phase and rutile catalysts, additional deep hydrogenated products such as CPOL and THFOL are also formed. With the exception of RTS catalyst,

FOL is completely consumed in reaction over other mixed and rutile samples with a remarkable conversion of 100%. The difference in acidic sites on RTS catalyst is evident from its NH_3-TPD data, showing shift in distribution from strong to moderate acidic sites.

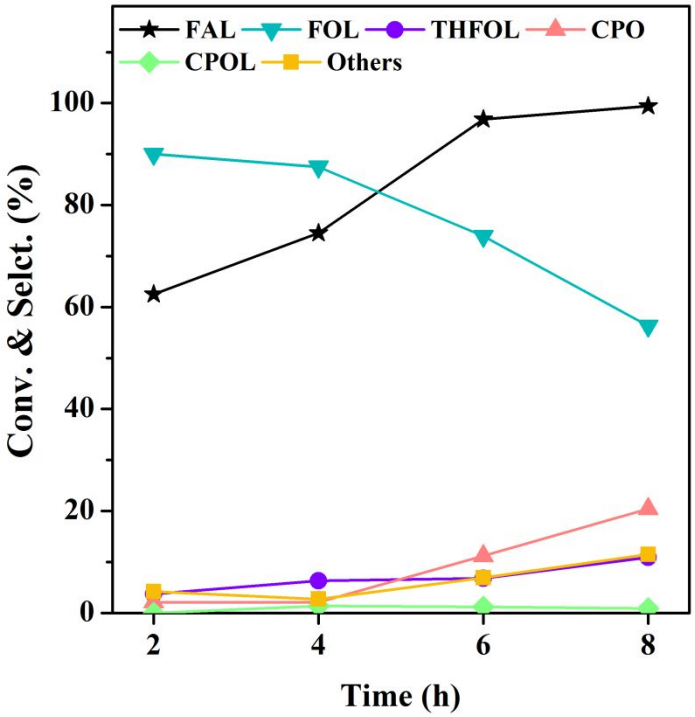

Figure 8. Furfural hydrogenation over RTH catalyst with respect to time. Reaction conditions: 5.2 mmol furfural, 50 mL water, 50 bar H_2, 100°C, 4h, 500 rpm.

The similarity in the activity over these catalysts can be understood from their H_2-TPR and NH_3-TPD experiments, where the Ni species and acidic sites profiles are similar for both mixed phase and rutile catalysts and are clearly distinguishable from pure anatase supported catalysts. Earlier reports have shown that the activation of carbonyl bond occurs on oxide surfaces[50,51]. Baker et. al observed that the FAL adsorption on titania surface generates furfuryl-oxy intermediate and it further hydrogenated at supported metal site. From DFT studies it was found that such adsorption is energetically favoured at oxygen vacant sites and is accompanied by charge transfer process[52]. The XPS results in present work clearly show that the all-titania catalysts contain certain amount of defect sites (Table S3). In addition, as the reaction is taking place in aqueous medium under high H_2 pressure and temperature, the

View Article Online
DOI: 10.1039/D3SE00131H

hydrogen molecules dissociated on Ni near to metal-support interface, can make these active sites available for furfural adsorption. But compared to mixed and rutile phase catalysts, the higher reducibility of anatase supports is found to be detrimental for FAL hydrogenation.

Most of the formed FOL on anatase catalysts due to higher amount acid sites undergo rearrangement to CPO. On the other hand, rutile catalysts comparatively have lesser amount of acidic sites, which lead to decrease in selectivity for CPO with the formation of THFOL as additional product at metal sites. The absence of THFOL (<0.5%) formation on anatase catalysts suggest that active sites for ring adsorption have been blocked. Cui et al. found that anatase support encapsulated Ni nanoparticles at 350°C, whereas such encapsulation can occur on rutile supports only at high temperature reduction (650°C)[40,53]. In our case, both anatase catalysts shows low activity compared to rutile catalysts, but at the reaction temperature of 140°C furfural conversion has reached 63.1 and 83.2% on ATH and ATA catalysts, respectively. Such high activities suggest that Ni sites are available for reaction to take place and are not completely blocked. XPS results have also shown that the binding energy is lower for Ni on anatase, suggesting redistribution of electron charge density between metal and support.

To investigate the possible impact of charge density on the reaction, the DFT studies were carried out on Ni clusters. The adsorption and energy barriers were calculated for electronically neutral and a charged (-1 electronic charge) Ni clusters. It is found that co-adsorption energy (Figure S6) of furfural and hydrogen has increased from -4.08 eV on neutral cluster to -4.73 eV on charged cluster. FAL and hydrogen separately have adsorption energy of -2.98 and -1.67 eV on neutral cluster, whereas -3.40 and -1.90 eV on charged cluster, respectively. These values suggest that excess charge on Ni can strengthen adsorption of molecules. The hydrogenation of carbonyl group can take place through two possible pathways (Figure S7), either by (a) adding first hydrogen to carbon, followed by addition of

View Article Online
DOI: 10.1039/D3SE00131H

second hydrogen to oxygen or (b) vice versa. Among them, the route (a) has lower energy barriers on both Ni clusters. The Ni cluster with excess electronic charge has higher hydrogenation barriers than on neutral cluster. Hence, the charge redistribution of Ni on anatase supports can affect the overall activity.

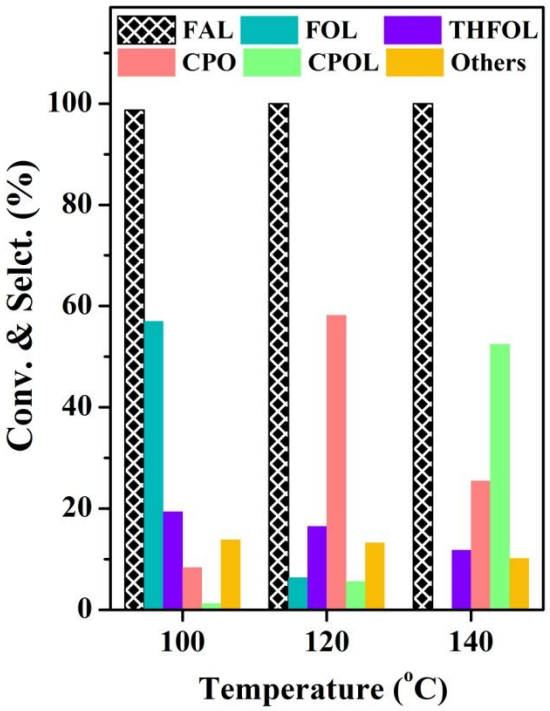

Figure 9. Furfural hydrogenation over RTH(10) catalyst at different temperatures. Reaction conditions: 5.2 mmol furfural, 50 mL water, 50 bar H_2, 4h, 500 rpm.

The product selectivity for CPOL on anatase catalyst is observed *ca.* 1%. Inspite of significant reaction observed for C=O group of FAL, the carbonyl of CPO molecule remains inactive. As given in Figure S7a and c, although the low energy barriers for carbonyl hydrogenation of CPO than FAL suggest that reaction is favourable, our results have also shown that adsorption strength of CPO on Ni cluster (-2.17 and -2.40 eV on neutral and charged cluster) is weaker than both FAL (given above) and FOL (-2.62 and -2.92 eV on neutral and charged cluster). This is further investigated by varying Ni content to 10 wt% on RH support, labelled as RTH(10).XRD pattern given in Figure S9 clearly shows complete reduction of Ni. RTH(10) catalyst activity at different temperatures with 10 wt% Ni content is

View Article Online
DOI: 10.1039/D3SE00131H

shown in Figure 9. In comparison with 5wt% Ni (RTH catalyst) the conversion at higher Ni content reaches to 98.7% even at 100°C. But higher conversion decreases selectivity of FOL to 57%. It is mainly converted to THFOL. The selectivity to CPO is nearly half of the ring hydrogenated product (8.4%). At higher temperature, FOL completely consumed after 4h to form CPOL as major product. Ring rearrangement products combinedly account for 78% selectivity. It was also observed that ring hydrogenation gets lightly suppressed at elevated temperatures. On comparing FOL and CPOL selectivity at 120 and 140°C, it is clear that until FAL or FOL is present in reaction solution, the adsorption and further reaction of CPO cannot be attained. Similar observations were made by Zhou et al. for Ni catalyst, where CPOL product was appeared only at higher Ni loading or at longer reaction time[54]. It is also applicable to anatase catalysts where significant amount of both FAL and FOL exist in reaction solution even at 140°C after 4h. Similarly, the weaker adsorption of FOL (-2.62 and -2.92 eV on neutral and charged Ni cluster) than FAL on Ni and presence of significant amount of unreacted FAL in reaction solution prevent FOL ring hydrogenation on anatase catalysts. On other hand, complete conversion of FAL on rutile catalysts allows adsorption of FOL to form THFOL.

The Ni leaching of all catalysts (Table S4) in reaction mixture after 4h remain below 3 ppm. The FTIR spectra of dried catalysts after reaction at 140°C (Figure S10) shows decrease in adsorbed furfural or formed intermediates/products on rutile compared to anatase supported catalysts. The reusability test was conducted over five runs using RTH catalyst. After every run, the catalyst was recovered and reused for next run. As shown in Figure S11, the furfural conversion and selectivity towards ring rearrangement and ring hydrogenation products during five recycles remain almost stable without any significant loss. The catalyst was characterized after 5 cycles and the resulting XRD is shown in Figure S12. As seen, although

View Article Online
DOI: 10.1039/D3SE00131H

there is an increase in the nickel crystallite size in the spent catalyst, the reaction results show that the both conversion and selectivity are retained, showing that the catalyst is robust.

Tolek et al. reported that Ru/TiO_2 catalysts with anatase phase have shown stronger interaction between metal and support than rutile phase, which lead to selective activation of carbonyl group at $Ru\text{-}TiO_x$ interface sites on anatase support and higher catalytic activity for FAL hydrogenation in alcohol medium[28]. Similarly on Pt/TiO_2 catalysts, the anatase support was active in aqueous phase, but FOL has further undergone rearrangement to CPO with higher selectivity on rutile support[55]. Compared to recent reports on Ni/TiO_2 catalysts, the catalysts in present study exhibited remarkable activity even at lower Ni content[30,31]. Chen et al. have suggested synergistic role of Ni-NiO heterojunction on P25 for furfural adsorption and hydrogenation[31]. The furfural conversion over RTH catalyst reduced using hydrazine method shows lower conversion (42.9%) than impregnated catalyst reduced under H_2 flow (Figure S13). This suggests that the reaction over RTH catalyst prepared by impregnation method involve additional active sites along with metal sites. The XRD pattern of our catalyst (shown in Figure S1) clearly shows absence of NiO in all catalysts. However, the XPS results shows formation of Ni-NiO surface during transfer of sample for analysis. Therefore role of Ni-NiO heterojunction cannot be discarded completely. To understand the role of support, the H_2-TPR of ATH and RTH catalyst was compared with their bare supports. Both phases of the support show different reducibility behaviour. As shown in Figure S14, the TPR profile of bare anatase titania support (AH) shows peak around 680°C. After loading with Ni precursor, the high temperature peaks were observed at 610 and 718°C. On other hand, the peak observed at 620°C on bare rutile support (RH) shifted to lower temperature after Ni loading and observed as shoulder at around 591°C. In order to provide further insight of the reduced catalyst, we have also performed Raman studies. As seen from Figure S15 ATH catalyst has shown a intense peak at 147 cm^{-1} characteristic of anatase E_g symmetry, whereas rutile (RTH)

View Article Online
DOI: 10.1039/D3SE00131H

sample show peaks at 430 and 600 cm^{-1}.[56-57] Along with the characteristic peaks for anatase, in ATH catalysts, we have a peak at 226 cm^{-1} corresponding to $NiTiO_3$ is also seen.[58] It is already established that Ni can replace some portion of Ti^{4+} ions particularly in anatase case so as to form $NiTiO_3$, since Ni^{2+} (0.72 Å) and Ti^{4+} (0.68 Å) has similar radius and there are huge number of defective sites in anatase support compared with rutile.[58] Since the amount of $NiTiO_3$ formed is very less we could not detect it in the XRD. However, in rutile catalysts peak corresponding to $NiTiO_3$ is not observed. On the other hand, NiO peak around 1060 to 1090 cm^{-1} was observed in both catalysts.[59] The origin of this NiO peak in sample is due to the overexposure of the sample to atmosphere. Also, the formation of $NiTiO_3$ in ATH sample is further supported by presence of high temperature (~718°C) TPR peak after Ni loading, which can be partially responsible for decrease of furfural conversion on anatase samples.

In present work, Ni supported either on mixed phase or rutile phase titania were found to be active than Ni supported on anatase phase support. Our results also suggest that in addition to active metal surface, the metal-support interface play a key role in determining overall activity of a catalyst, as it can anchor and activate furfural through carbonyl for hydrogenation. The availability of metal sites, charge on metal and acidity further tunes product selectivity. The present studies clearly demonstrate how phase composition of titania support was able to tune nature of metal through metal-support interaction and acidic sites for furfural hydrogenation.

Conclusions

Ni catalysts supported on anatase, rutile and mixed phase TiO_2 were developed for selective hydrogenation of furfural in aqueous medium. The support phase of Ni/TiO_2 catalysts modulates the metal-support interaction effecting both activity and the product distribution of the reaction. It is evident from H_2-TPR that titania with mixed and rutile phase interact Ni nanoparticles strongly than anatase supports. The XPS results indicated significant charge

redistribution between Ni and anatase support. Pure anatase supported Ni catalysts have shown lower activity than rutile containing catalysts, but higher selectivity for furfuryl alcohol and cyclopentanone depending on reaction temperature. The additional deep hydrogenation products like tetrahydrofurfuryl alcohol and cyclopentanol are found only on rutile and mixed phases catalysts. Finally, the differences in the selectivity are explained by using the DFT studies, which suggest that the adsorption strength of active species on Ni metal influenced the final product that is formed in the reaction. The results clearly illustrate the role of metal-support interaction and crystal phase on both activity and product distribution. This work paves way for new insights into rational design of catalysts for direct conversion of initial stage platform biomass chemicals to value added products.

ACKNOWLEDGMENTS

The authors gratefully acknowledge the support of the Department of Science and Technology (DST), India, for funding the National Centre for Catalysis Research (NCCR). The authors also acknowledge the High Performance Computing Environment (HPCE), Indian Institute of Technology Madras for providing computational facilities. The authors are grateful to Prof. Ch. Subrahmanyam, Department of Chemistry, Indian Institute of Technology Hyderabad for supporting us with TPR and TPD data. We acknowledge Nanotechnology Research Centre (NRC), SRMIST for providing the research facilities.

AUTHORS INFORMATION

Corresponding Authors

View Article Online
DOI: 10.1039/D3SE00131H

1. Prof. Madhavan Jaccob

ORCID iD: 0000-0002-2632-4076

*E-mail: madhavanjack05@gmail.com

2. Prof. Krishnamurthy Konda Ramaswamy

*E-mail: krkonda1949@gmail.com

3. Prof. Balasubramanian Viswanathan

ORCID iD: 0000-0002-8857-7271

*E-mail: bviswanathan@gmail.com

Supplementary Information

The Supplementary Information includes catalysts synthesis procedures, characterization details, catalytic activity test procedures, computational details, SEM-EDX images, Tables, Figures and Cartesian coordinates.

CONFLICT OF INTEREST

The authors have declared no conflict of interest.

REFERENCES

(1) F. H. Isikgor and C. R. Becer, Polym. Chem., 2015, **6 (25)**, 4497–4559.

(2) G. Haarlemmer, C. Guizani, S. Anouti, M. Déniel, A. Roubaud and S. Valin, *Fuel*, 2016, **174**, 180–188.

(3) X. Zhang, K. Wilson and A. F. Lee, *Chem. Rev.*, 2016, **116 (19)**, 12328–12368.

(4) F. Delbecq, Y. Wang, A. Muralidhara, K. E. Ouardi, G. Marlair and C. Len, *Front. Chem.*, 2018, **6**, 146.

(5) J. M. R. Gallo, J. M. C. Bueno and U. Schuchardt, *J. Braz. Chem. Soc.,* 2014, **25**, 2229–2243.

(6) X. Wang, X. Liang, P. Geng and Q. Li, *ACS Catal.,* 2020, **10 (4)**, 2395–2412.

(7) M. Tamura, Y. Nakagawa and K. Tomishige, *J. Japan Pet. Inst.,* 2019, **62 (3)**, 106–119.

(8) M. Kabbour and R. Luque, in *Biomass, Biofuels, Biochemicals: Recent Advances in Development of Platform Chemicals*, ed. S. Saravanamurugan, A. Pandey, H. Li and A. Riisager, Elsevier, Amsterdam, 2019, ch. 10, pp. 283–297.

(9) H. Chen, J. Ding, H. Liang and H. Yu, *ChemistrySelect*, 2020, **5 (13)**, 4085–4090.

(10) A. Szczurek, V. Fierro, M. Thébault, A. Pizzi and A. Celzard, *Eur. Polym. J.,* 2016, **78**, 195–212.

(11) M. Modelska, M. J. Binczarski, P. Dziugan, S. Nowak, Z. Romanowska-Duda, A. Sadowski and I. A. Witońska, *Energies*, 2020, **13 (24)**, 6684.

(12) X. Liu, B. Zhang, B. Fei, X. Chen, J. Zhang and X. Mu, *Faraday Discuss.,* 2017, **202**, 79–98.

(13) D. Belsito, D. Bickers, M. Bruze, P. Calow, M. L. Dagli, W. Dekant, A. D. Fryer, H. Greim, Y. Miyachi, J. H. Saurat and I. G. Sipes, *Food Chem.Toxicol.*, 2012, **50 (3)**, S517-S556.

(14) Y. Nakagawa, H. Nakazawa, H. Watanabe and K. Tomishige, *ChemCatChem*, 2012, **4 (11)**, 1791–1797.

(15) X. Meng, Y. Yang, L. Chen, M. Xu, X. Zhang and M. Wei, *ACS Catal.*, 2019, **9 (5)**, 4226–4235.

(16) S. K. Vatti, K. K. Ramaswamy and V. Balasubramanaian, *J. Adv. Nanomater.*, 2017, **2 (2)**, 127-132.

(17) X. Zhang, P. Yan, B. Zhao, K. Liu, M. C. Kung, H. H. Kung, S. Chen, Z. C. Zhang, *ACS Catal.*, 2019, **9 (4)**, 3551–3563.

(18) S. Bernal, J. J. Calvino, M. A. Cauqui, J. M. Gatica, C. Larese, J. A. Pe, Â. Omil and J. M. Pintado, *Catal. Today*, 1999, **50 (2)**, 175-206.

(19) M. Abid and R. Touroude, *Catal. Lett.*, 2000, **69**, 139-144.

(20) P. Sudarsanam, H. Li and T. V. Sagar, *ACS Catal.*, 2020, **10 (16)**, 9555–9584.

(21) A. M. Ruppert, J. Grams, M. Jędrzejczyk, J. Matras-Michalska, N. Keller, K. Ostojska, P. Sautet, *ChemSusChem*, 2015, **8 (9)**, 1538–1547.

(22) C. Hernandez-Mejia, E. S. Gnanakumar, A. Olivos-Suarez, J. Gascon, H. F. Greer, W. Zhou, G. Rothenberg and N. Raveendran Shiju, *Catal. Sci. Technol.*, 2016, **6 (2)**, 577–582.

(23) B. Seemala, C. M. Cai, C. E. Wyman and P. Christopher, *ACS Catal.*, 2017, **7 (6)**, 4070–4082.

(24) J. Xu, Q. Cui, T. Xue, Y. Guan and P. Wu, *ACS Omega*, 2020, **5 (46)**, 30257–30266.

(25) H. Rojas, J. J. Martínez and P. Reyes, *Dyna (Medellin)*, 2010, **77**, 151-159.

(26) M. Pirmoradi, R. J. Gulotty and J. R. Kastner, *Catal. Sci. Technol.*, 2020, **10 (20)**, 7002–7015.

(27) R. Rodiansono, M. D. Astuti, S. Khairi and S. Shimazu, *Bull. Chem. React. Eng. Catal.*, 2016, **11**, 1–9.

(28) W. Tolek, N. Nanthasanti, B. Pongthawornsakun, P. Praserthdam and J. Panpranot, *Sci. Rep.*, 2021, **11 (1)**, 9786.

(29) B. Chen, F. Li, Z. Huang and G. Yuan, *Appl. Catal. A Gen.*, 2015, **500**, 23–29.

(30) Y. Li, X. Guo, D. Liu, X. Mu, X. Chen and Y. Shi, *Catalysts*, 2018, **8 (5)**, 193.

(31) S. Chen, T. T. Qian, L. L. Ling, W. Zhang, B. B. Gong and H. Jiang, *ChemSusChem*, 2020, **13 (20)**, 5507–5515.

(32) M. Przydacz, M. Jędrzejczyk, M. Brzezińska, J. Rogowski, N. Keller, A. M. Ruppert, *J. Supercrit. Fluids*, 2020, **163**, 104827.

(33) M. M. Mahlambi, A. K. Mishra, S. B. Mishra, R. W. Krause, B. B. Mamba and A. M. Raichur, *J. Therm. Anal. Calorim.*, 2012, **110**, 847–855.

(34) R. A. Spurr and H. Myers, *Anal. Chem.*, 1957, **29 (5)**, 760-762.

(35) X. Zhang, P. Yan, B. Zhao and Z. C. Zhang, *Catal. Sci. Technol.*, 2021, **11 (1)**, 297–311.

(36) M. Hronec, K. Fulajtárova and T. Soták, *Appl. Catal. B: Environ.*, 2014, **154–155**, 294–300.

(37) Z. Yu, H. Tian, K. Sun, Y. Shao, L. Zhang, S. Zhang, P. Duan, Q. Liu, S. Niu, D. Dong and X. Hu, *Mol. Catal.*, 2020, **496**, 111187.

(38) S. Nandi, A. Saha, P. Patel, N. H. Khan, R. I. Kureshy and A. B. Panda, *ACS Appl. Mater. Interfaces*, 2018, **10**, 29, 24480–24490.

(39) Y. Shao, K. Sun, L. Zhang, Q. Xu, Z. Zhang, Q. Li, S. Zhang, Y. Wang, Q. Liu and X. Hu, *Green Chem.*, 2019, **21 (24)**, 6634–6645.

(40) J. Zhang, Y. Wang, C. Zhang, H. Gao, L. Lv, L. Han and Z. Zhang, *ACS Sustain. Chem. Eng.*, 2018, **6 (2)**, 2231–2239.

(41) B. Cui, H. Wang, J. Han, Q. Ge and X. Zhu, *J. Catal.*, 2022, **413**, 880–890.

(42) N. S. Resende, C. A. Perez, J. G. Eon and M. Schmal, *Catal. Lett.*, 2011, **141 (11)**, 1685–1692.

(43) J. Jae, W. Zheng, R. F. Lobo and D. G. Vlachos, *ChemSusChem*, 2013, **6 (7)**, 1158–1162.

(44) R. Rios-Escobedo, E. Ortiz-Santos, J. A. Colín-Luna, J. N. Díaz de León, P. del Angel, J. Escobar and J. A. de los Reyes, *Top. Catal.,* 2022, **65(13–16)**, 1448–1461

(45) H. Chen, H. Ruan, X. Lu, J. Fu, T. Langrish and X. Lu, *Mol. Catal.*, 2018, **445**, 94–101.

(46) Z. Zhao, R. Bababrik, W. Xue, Y. Li, N. M. Briggs, D. T. Nguyen, U. Nguyen, S. P. Crossley, S. Wang, B. Wang and D. E. Resasco, *Nat. Catal.*, 2019, **2 (5)**, 431–436.

(47) M. Hronec and K. Fulajtarová, *Catal. Commun.*, 2012, **24**, 100–104.

(48) N. Pino, G. Hincapié and D. López, *Ing. Investig.*, 2017, **37 (1)**, 34–42.

(49) T. Shen, R. Hu, C. Zhu, M. Li, W. Zhuang, C. Tang and H. Ying, *RSC Adv.*, 2018, **8 (66)**, 37993–38001.

(50) G. Kennedy, L. R. Baker and G. A. Somorjai, *Angew. Chem. Int. Ed.*, 2014, **53 (13)**, 3405–3408.

(51) G. Kennedy, G. Melaet, H. L. Han, W. T. Ralston and G. A. Somorjai, *ACS Catal.*, 2016, **6 (10)**, 7140–7147.

(52) L. R. Baker, G. Kennedy, M. van Spronsen, A. Hervier, X. Cai, S. Chen, L. W. Wang and G. A. Somorjai, *J. Am. Chem. Soc.*, 2012, **134 (34)**, 14208–14216.

(53) B. Cui, H. Wang, Q. Ge and X. Zhu, *Catalysts*, 2022, **12 (9)**. 955.

(54) M. Zhou, H. Zhu, L. Niu, G. Xiao and R. Xiao, *Catal. Lett.*, 2014, **144 (2)**, 235–241.

(55) M. Y. Byun, Y. E. Kim, J. H. Baek, J. Jae and M. S. Lee, *RSC Adv.*, 2022, **12 (2)**, 860–868.

(56) S. Challagulla, K. Tarafder, R. Ganesan and R. Sounak, *Sci. Rep.*, 2017, **7**, 8783.

(57) V. Swamy and B. C. Muddle, *Appl. Phys. Lett.*, 2006, **89**, 163118.

(58) I. Ganesh, A. K. Gupta, P. P. Kumar, P. S. C. Sekhar, R. Radha, G. Padmanabham and G. Sundararajan, *Sci. World J.*, 2012, DOI: 10.1100/2012/127326.

(59) A. Y. Faid, A. O. Barnett, F. Seland and S. Sunde, *Electrochim. Acta*, 2020, **361**, 137040.

View Article Online
DOI: 10.1039/D3SE00131H